





Electromagnetic Behavior of Cu and Ni Nanofilms in the X-band

Vitor Fernando de Melo Gonçalves¹ , Erick Gabriel Ribeiro dos Anjos¹ , Guilherme Ferreira de Melo Morgado¹ , Tayra Rodrigues Brazil¹ , Maurício Ribeiro Baldan² , Maria Aparecida Miranda de Souza³ , Evandro Luís Nohara⁴ , Mirabel Cerqueira Rezende^{1,*} 

1. Universidade Federal de São Paulo  – Instituto de Ciência e Tecnologia – Laboratório de Tecnologia de Polímeros e Biopolímeros — São José dos Campos/SP – Brasil. **2.** Instituto Nacional de Pesquisas Espaciais  – Laboratório Associado de Sensores e Materiais – São José dos Campos/SP – Brasil. **3.** Departamento de Ciência e Tecnologia Aeroespacial  – Instituto de Aeronáutica e Espaço – Divisão de Materiais – São José dos Campos/SP – Brasil. **4.** Universidade de Taubaté  – Departamento de Engenharia Mecânica – Taubaté/SP – Brasil.

*Correspondence author: mirabel.rezende@unifesp.br

ABSTRACT

Currently, the presence of spurious microwave radiation is increasing in the environment, which has caused concern due to possible health problems in living beings and electromagnetic interference in electronic systems. To control this problem, studies in the materials area are taking place, aiming to attenuate the spurious radiation and meet requirements of good performance in broadband, low cost and low weight. The present work aimed to study Cu and Ni nanometric films with thicknesses of 65 and 200 nm, deposited on polyethylene terephthalate substrate by magnetron sputtering. Scanning electron microscopy with a field emission gun (FEG-SEM) showed that the films produced have different morphological textures, due to the parameters used in the sputtering process and also the free energy of metals. Impedance spectroscopy measurements showed that the films have low conductivity values, due to the metallic oxides formed on the film surfaces, confirmed by X-ray diffraction, and also to the presence of defects. Electromagnetic characterization (8.2 – 12.4 GHz) showed that the Cu and Ni thin films had low performance, except the Ni_200 nm film, which showed a total shielding efficiency of about 30% in broadband. This result is promising considering the nanometric thickness of the Ni film.


Keywords: Electromagnetic shielding; Energy absorption films; Thin films; Nickel coatings; Copper; Magnetron sputtering.

INTRODUCTION

Nowadays, the deposition of thin films on polymeric substrates is a technology that is being studied more widely due to their application in different areas involving innovations in the sectors of special packaging, military, solar cells, sensors, telecommunication, microelectronics, and optics (Abdumutalibovich 2021; Cordill *et al.* 2022; Kumar 2019; Ohring 2001; Soethe *et al.* 2011).

The literature shows that nanometer thin films deposited on suitable substrates exhibit different physical characteristics than those exhibited by micro and millimetric films or bulk materials (Hsu *et al.* 2018; Ohring 2001; Naghdi *et al.* 2018; Soethe *et al.* 2011). The consulted literature shows various studies involving thin films, for example, simulations performed to investigate the mechanical properties of Cu/Zr multilayer nanofilms during tensile and compression tests, where the authors observed the slipping behavior in the tensile test for the Cu film and the phase transformation process in the compression test for the Zr film

Received: Mar 14, 2023 | Accepted: May 04, 2023

Section editor: Mariana Fraga 

Peer Review History: Single Blind Peer Review.



This is an open access article distributed under the terms of the Creative Commons license.

(Hsu *et al.* 2018). Goktas S and Goktas A (2021), show an interesting study involving the production of ZnO films based on heterojunction/nanocomposite photocatalysts. This material gets great attention due to its possible contribution to solving the crises of energy supply and promoting the degradation of various pollutants, but the fabrication techniques of this class of material can play crucial tasks, which complicate the material obtaining. Goktas A (2018), studied also thin films of Co and Cu co-doped ZnO evaluating the effects of air and argon annealing environments, and observed increased Cu doping levels in the samples sintered in argon. Luo *et al.* (2023), describe the obtaining of graphene nanofilms with thicknesses varying from 50 to 600 nm, with relevant results of electromagnetic shielding mainly by reflection, due to the great electrical conductivity of the graphene, but with little contribution by absorption, which limits their application as radar absorbing material (RAM).

RAM and materials for electromagnetic (EM) shielding have numerous applications, stand out the control of spurious radiation in automotive and aerospace industries, in military technology, as well as in wireless electrical and electronic devices and communication systems, highlighting an environment free of harmful radiation for living beings (Abhishek and Singh 2018; Biscaro *et al.* 2008; Bregar 2004; Folgueras and Rezende 2007; Hashish 2002; Kumar and Vadera 2017; Nie *et al.* 2007; Rezende *et al.* 2000). Considering the increasingly tighter requirements in these areas, new challenges always arise in the search for materials with good performance in attenuating EM radiation in a wide range of frequencies, with low cost, low weight, and easy application.

Among the materials capable of attenuating the energy of the incident EM wave, we can mention ferrites (Nie *et al.* 2007; Pinto *et al.* 2019; Reis *et al.* 2022; Silveira *et al.* 2020), carbon materials (for example, carbon black, carbon nanotubes, and graphene) (Anjos *et al.* 2023; Ruiz-Perez *et al.* 2022; Vieira *et al.* 2021; Wang *et al.* 2021a), conductive polymers (Biscaro *et al.* 2008; Pinto *et al.* 2018; Pinto and Rezende 2018), and thin films (Abdumutalibovich 2021; Naghdi *et al.* 2018; Soethe *et al.* 2011). In the latter area cited, the literature presents, for example, metallic thin films based on Kanthal with thickness varying from 10 to 200 nm, which can behave as microwave absorbing material, when used as a coating on inner walls of waveguides with the advantage to be much lighter (Bhat *et al.* 1998; Soethe *et al.* 2011).

These materials, independent of this physicochemical nature, can differ in their internal mechanisms of energy transformation, but basically, the intensity of the EM wave is attenuated through loss processes based on the dissipation of the incident radiation energy in heat, by the Joule effect or interference-dispersed microwave (Saleem *et al.* 2020).

The materials that interact with the magnetic field of the EM wave are called magnetic absorbing materials, for example, those based on ferrites and magnetic materials (Dias *et al.* 2012; Gama and Rezende 2010; Nie *et al.* 2007; Pinto *et al.* 2017; Pinto *et al.* 2019; Silveira *et al.* 2017; Yadav and Panwar, 2022). On the other hand, materials that interact with the electric field of the EM wave are known as dielectrics, which can be cited as those based on carbon materials (Rojas *et al.* 2021; Ruiz-Perez *et al.* 2022), conductive polymers (Pinto *et al.* 2018), and dielectric thin films (Abdumutalibovich 2021; Naghdi *et al.* 2018; Parucker *et al.* 2022). RAM can also be classified as hybrid material when it combines magnetic and dielectric characteristics.

Besides the great efforts in the area of RAM, it is still a great challenge to develop a novel EM wave absorbers which simultaneously satisfy all the necessities such as broad and strong absorption bandwidth in a wide frequency range, small thickness, and light-weight (Saleem *et al.* 2020). Aiming to reach these challengers, the consulted literature shows an increased interest in the area of metallic thin films for use as RAM or as shielding materials. Costa *et al.* (2017) prepared thin films of Al (20 – 80 nm) and Cu (20 – 100 nm) obtained by magnetron sputtering with attenuation values below 3 dB. Parucker *et al.* (2022) studied Ti thin films (20 – 100 nm) with results of < 3 dB and Silva and Ferreira (2019) characterized Ti thin films with different purities and obtained values below 3 dB for TiGr2 (2.0 -7.5 nm) and ~8 dB for TiGr5 (4 nm). Soethe *et al.* (2011) studied also Ti thin films (20 - 100 nm) produced by magnetron sputtering and found values of attenuation below 3 dB. Considering that 3 dB corresponds to almost 50% of the incident wave attenuation, these results show a good potential to be used in hybrid and composite materials with the great advantage of reduced thickness and weight.

Thus, given the increasing use of EM shielding materials in recent years, nanomaterials have found much attention as exceptional EM wave absorption materials due to their high surface energy and small size (Saleem *et al.* 2020). In this context, metallic thin films are light materials, easy to apply and with potential to be used as RAM. So, this study was motivated to be carried out with the objective of studying the electrical and electromagnetic properties of copper and nickel thin films with 65 and 200 nm, produced by magnetron sputtering. The EM behavior of the films was evaluated in the frequency range of 8.2 to 12.4 GHz.

MATERIALS AND METHODS

Materials

This study used metallic targets of nickel (magnetic material) and Cu (dielectric material), both with a purity of 99.99% and diameter of 152.4 mm, from Curtis Instruments Co. and a flexible substrate of the poly(ethylene terephthalate) (PET) (Mylar®), with 0.07 mm of thickness. This substrate is tear resistant and with good thermal stability (until ~230 °C).

Film Deposition

The thin films were obtained by deposition of the Cu and Ni metals on the PET substrate with thicknesses of 65 and 200 nm, by magnetron sputtering technique, using a plasma reactor constructed by the authors, based on the literature works (Fontana and Muzart 1998; Soethe *et al.* 2011). Figure 1 shows the used equipment. The studied thicknesses were defined based on the skin depth of the samples, knowing that above the skin depth the samples become reflectors.



Figure 1. Plasma reactor used in this study.

Before the deposition of the monolayer thin films of Cu and Ni with different thicknesses (65 and 200 nm), the system was evacuated to a pressure of 0.04 mTorr, and argon gas was injected up to a working pressure of 40 mTorr. The metallic target was positioned 300 mm from the PET substrate. The deposition rate was chosen so as to maintain a homogeneous film deposition on PET. Table 1 shows the experimental parameters (voltage, current, and deposition rate) used in the deposition of the nanometric metallic films.

Table 1. Experimental parameters used in the deposition of the monolayer Cu and Ni thin films.

Film	Thickness (nm)	Current (A)	Voltage (V)	Deposition rate (nm/s)
Cu_65	65	2.0	549	0.50
Cu_200	200	2.0	546	0.50
Ni_65	65	2.0	506	0.43
Ni_200	200	2.1	501	0.42

Source: Elaborated by the authors.

To avoid opening the reactor chamber during the deposition of metallic films and thus guarantee the same reactor conditions in all experiments, a sample holder was used with a continuous PET substrate feeding system. For this, the used plasma reactor has two different target supports, one for the Cu target and the other for the Ni, which is selected according to the film to be

deposited. The film thicknesses were monitored in real-time with a quartz crystal resonator, with the simultaneous deposition of metal on the PET substrate and also on the quartz crystal.

Characterization

Field emission gun scanning electron microscopy (FEG-SEM)

FEG-SEM was used to investigate the morphology of samples using a TESCAN - MIRA3 high-resolution scanning electron microscope assisted with a field emission gun, operating at 5 kV. The samples were positioned in stubs with carbon tape and coated with a thin layer of gold for 90 s in a sputtering Quorum, Q150RS Plus.

Energy dispersive X-ray spectroscopy (EDS)

EDS analyses of the metallic thin films and PET were performed in a FEI Inspect S50 microscopy coupled with a system to chemical microanalysis. The samples were previously coated with ~5 nm Au layer to avoid charging during the electron irradiation.

Atomic force microscopy (AFM)

AFM analyses of the metallic thin films and the PET substrate were performed in a Bruker/Dimension Icon AFM equipment. The scanning model was the ScanAsyst-Air with a silicon tip on the nitride cantilever, the frequency of 70 kHz and the spring constant of 0.4 N/m. The analyzed area of samples was 1 μm x 1 μm . The data were analysed using the NanoScope Analysis 1.8 tool.

X-ray diffraction (XRD)

The crystalline structure of the metallic thin films was evaluated by XRD in a Rigaku model Ultima IV X-ray diffractometer, at room temperature, with copper K α radiation ($\lambda = 1.54056 \text{ \AA}$) and a filter of Ni for the K β radiation. The measurements were carried out with a tension of 40 kV, an electrical current of 30 mA, and a scan speed of 10°/min in the angular region of 2 θ from 20 to 70°. The incidence angle was 0.5° for the Cu_200nm sample, 1.0° for the PET, Ni_65nm, and Ni_200nm, and 1.5° for the Cu_65nm films.

Impedance spectroscopy (IS)

The AC electrical conductivity of samples was investigated by IS (or dielectric spectroscopy) measurements. The analyses were performed in a Solartron SI 1260 impedance/gain-phase analyser at room temperature, with a tension of 0.5 V and in the frequency range of 1 to 10⁶ Hz, collecting 50 points. For these, two gold circular electrodes measurements were deposited (diameter of 6.68 mm and area (A) of 3.34x10⁻⁵ m²) by sputtering on parallel sides of samples. The complex impedance (Z^*), real impedance component (Z'), and imaginary impedance component (Z'') were obtained, considering the thicknesses of samples (d) of 0.07 mm (the same thickness as the PET substrate). From Z' and Z'' the AC electrical conductivity (σ_{AC}) was calculated, Eqs. 1–3 (Al-Saleh *et al.* 2013; Monti *et al.* 2021):

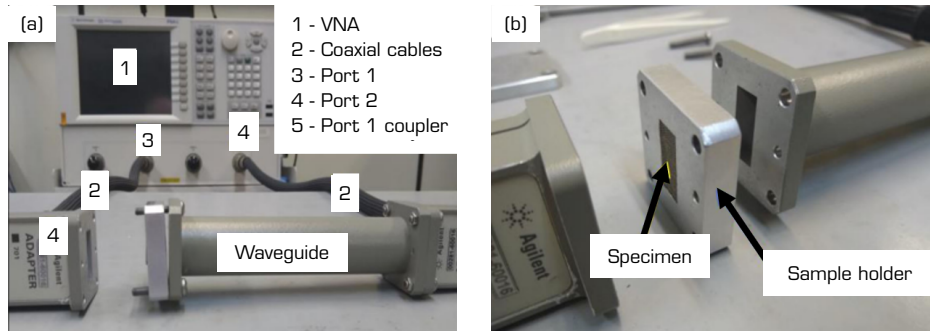
$$Z^* = Z' + iZ'' \quad (1)$$

$$|Z^*| = \sqrt{(Z')^2 + (Z'')^2} \quad (2)$$

$$\sigma_{AC} = \frac{d}{A |Z^*|} \quad (3)$$

Electromagnetic characterization

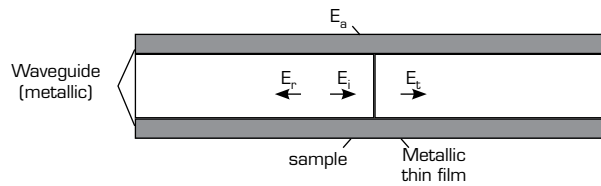
The electromagnetic characterization of the nanometric films was performed in a vector network analyzer (VNA, Agilent Technologies, model PNA-L N5235A) (Fig. 2a) using a waveguide (WR-90) in X-band, that is, in the frequency range of 8.2 – 12.4 GHz (Fig. 2b) and a software Agilent Technologies-85071E.



Source: Adapted from Ribeiro *et al.* (2021).

Figure 2. A two-port VNA used in the EM characterization (a); and the sample-holder and waveguide used in the X-band measurements (b).

From the scattering parameters (S-parameters) measured for all samples, it was calculated the absorbed (E_a), reflected (E_r), and transmitted (E_t) energies, considering the incident energy (E_i). Figure 3 shows schematically the setup used in these measurements.



Source: Adapted from Soethe *et al.* (2011).

Figure 3. Schematic of the waveguide settings used in the EM characterization: E_a – absorbed energy; E_r – reflected energy; E_i – incident energy; E_t – transmitted energy.

From the measured S-parameters, the values of reflection[®], transmission (T), and absorption (A) involved in the energy balance were calculated according to Eqs. 4–6 (Wang *et al.* 2021b). The complex parameters of the electrical permittivity (ϵ' and ϵ'') and the magnetic permeability (μ' , μ'') were also evaluated by the Nicolson-Ross-Weir model (Nicolson and Ross 1970).

$$R = |S_{11}|^2 \quad (4)$$

$$T = |S_{21}|^2 \quad (5)$$

$$A = 1 - R - T \quad (6)$$

The total shielding effectiveness (SE_T), reflection shielding effectiveness (SE_R), and absorption shielding effectiveness (SE_A) also were calculated, according to Eqs. 7–9, and expressed in decibels (dB) (Rajavel *et al.* 2020; Wang *et al.* 2021b).

$$SE_T = SE_R + SE_A \quad (7)$$

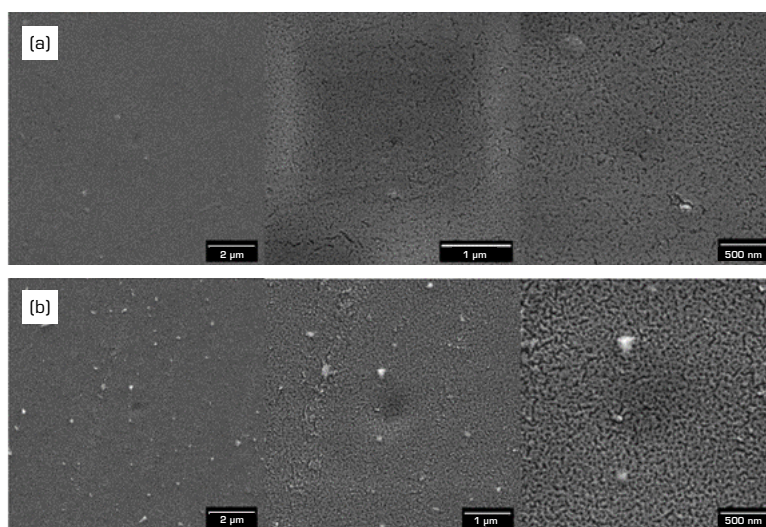
$$SE_R = -10(1 - R) \quad (8)$$

$$SE_A = -10 \left(\frac{T}{1-R} \right) \quad (9)$$

RESULTS AND DISCUSSION

Morphological characterization

Figure 4 shows the morphological aspects of the Cu thin films obtained by FEG-SEM, with thicknesses of 65 and 200 nm, respectively. Comparing these images, it is observed that the smooth surface of PET substrate with slight ripples and without cracks and larger defects, usually found for polymeric films, changed significantly after the magnetron sputtering process, confirming the Cu deposition on the polymeric substrate. Figure 4a shows the image of Cu thin film with 65 nm of thickness obtained in the lowest magnification (25,000x). This figure shows a layer of metal distributed over the entire PET surface. It is known that the metal film growth depends on the substrate-thin film material interaction, metal-metal interaction, and the growth conditions until a continuous film has recovered the whole substrate surface (Cordill *et al.* 2022).



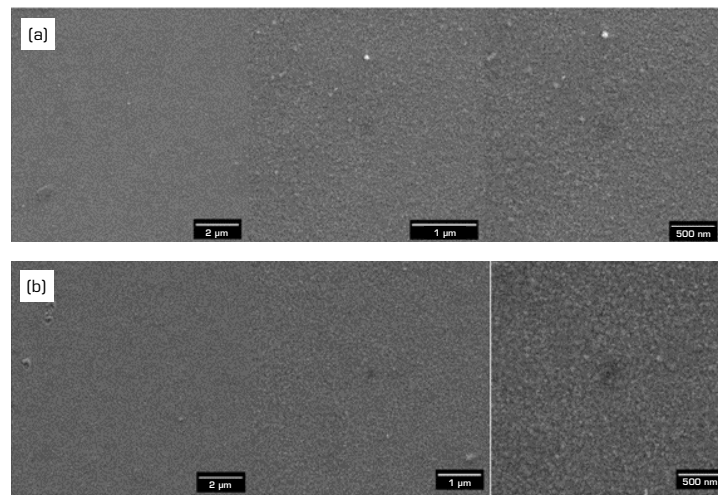
Source: Elaborated by the authors.

Figure 4. FEG-SEM of the nanometric films of Cu with 65 nm (a) and 200 nm (b) of thickness.

The analysis of the images obtained in higher magnifications (75,000x and 100,000x) shows with major detail the presence of rich regions in Cu and voids. Figure 4b shows images of the Cu thin films with 200 nm. These images show more homogeneous films recovering the entire PET surface, with porous but without striations. Comparatively, the Cu_65 sample is smoother than the Cu_200 film, but both are formed by islands surrounded by voids. The thicker film (200 nm) still presents some larger islands that stand out above the formed film surface. All samples analysed do not show delamination and cracks and these results are in agreement with the literature, which mentions that the Cu metal forms ductile films with good adhesion to the polymer substrate without the need of using adhesion interlayer systems (Cordill *et al.* 2022; Marx *et al.* 2015; Putz *et al.* 2017).

Figure 5a, b shows the morphological aspects of the Ni thin films with thicknesses of 65 and 200 nm, respectively, obtained by FEG-SEM. Figure 5a shows that the Ni_65 thin film presents a texture denser, fine, and more compact compared to the Cu_65 sample. A few defects are observed in some regions of the films, which can be attributed to previous impurities on the PET film.

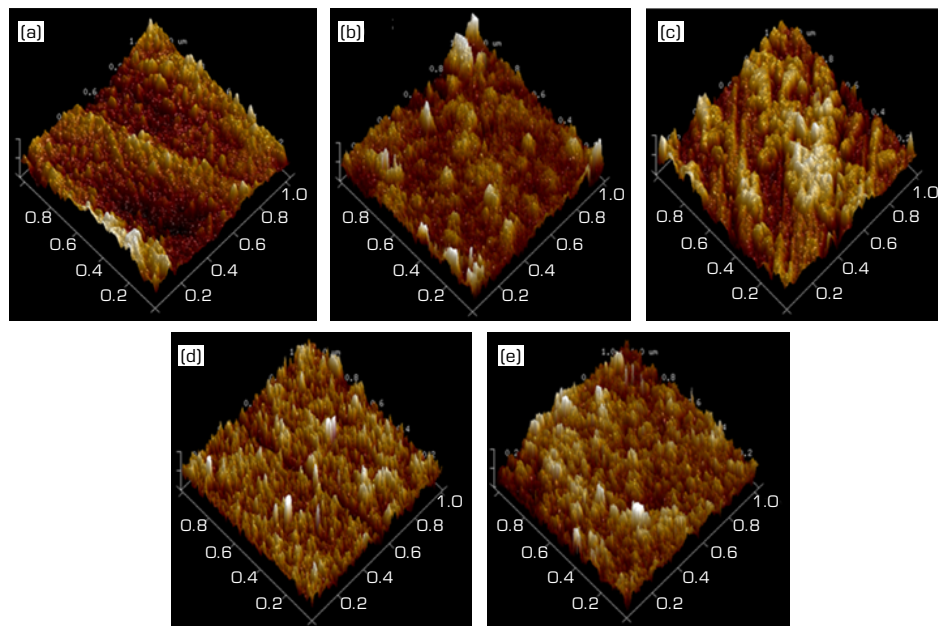
FEG-SEM images of the Ni thin films with 200 nm (Fig. 5b) show similar morphological aspects of the nanofilm with 65 nm. As can be seen, the metallic film was deposited homogeneously on the PET substrate, with the tendency to formation of islands, but without visible defects and agglomerates. These images show also the presence of nanovoids in both films with different thicknesses.



Source: Elaborated by the authors.

Figure 5. FEG-SEM of the nanometric films of Ni with 65 nm (a) and 200 nm (b) of thickness.

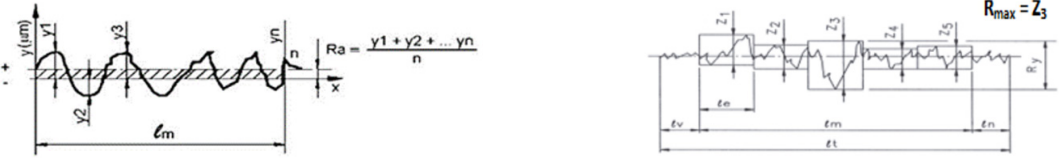
Figure 6 shows the morphological aspects of PET and the metallic thin films, with thicknesses of 65 and 200 nm, obtained by AFM analyses. These analyses show the effective surface (surface evaluated by a measurement technique, in this case, AFM). The PET film shows the presence of peaks and valleys (darker regions), probably due to the manufacturing process used to obtain this polymeric film. Table 2 shows its roughness with R_a values of 1.98 nm and R_{max} of 18.5 nm (R_a and R_{max} schematized in Table 2). The analysis of the images of the Cu films with 65 and 200 nm of thickness shows that the valleys observed in the PET substrate were filled by the Cu deposition and the first Cu peaks can be seen in the 65 nm sample. The Cu_200 sample has a denser metallic surface with the presence of some higher and smoother regions (lighter regions). The lower R_a values of Cu_65 in Table 2 confirm that Cu filled the valleys present in the PET substrate and the higher R_{max} indicates the formation of higher peaks of Cu. In accordance with the FEG-SEM analyses, the AFM images of the Ni films show a denser and thinner morphology, with fine peaks covering the entire surface of the polymeric substrate. First, the Ni_65 film shows the lower R_a measured (0.87 nm), due to the homogeneous recovery of the PET valleys by Ni deposition, followed by the formation of higher peaks (R_{max} of 26.3 nm).



Source: Elaborated by the authors.

Figure 6. AFM images of PET and the nanometric films of Cu and Ni with 65 nm and 200 nm of thickness. (a) PET; (b) Cu_65; (c) Cu_200; (d) Ni_65; (e) Ni_200.

Table 2. Roughness R_a and R_{max} of samples obtained by the AFM analyses.

Sample	R_a (nm)	R_{max} (nm)
		
PET	1.98	18.5
Cu_65	1.40	24.3
Cu_200	2.59	22.1
Ni_65	0.87	13.2
Ni_200	1.81	26.3

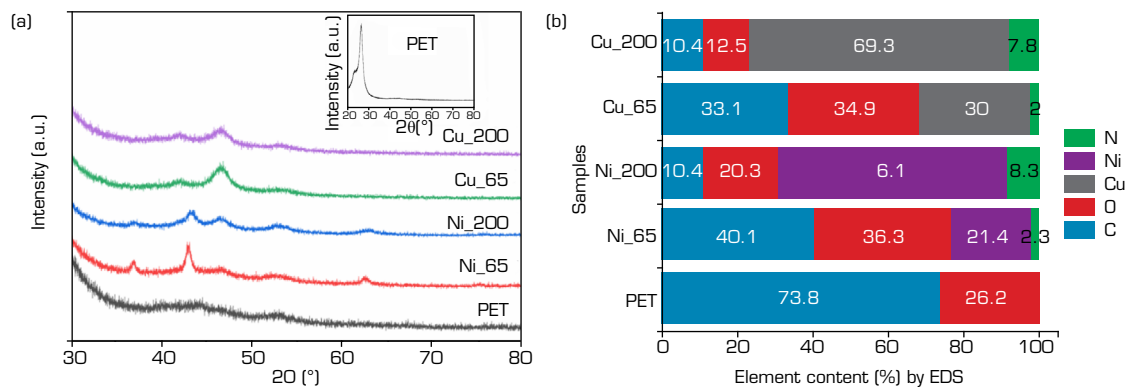
Source: Elaborated by the authors.

The continuous structure with the tendency to form more thin peaks (or islands) observed in the nanofilms of Ni can be attributed to the high free energy of nickel (2.364 J/m^2), which resulted in a denser film (Himpel *et al.* 1998). The comparison of Figs. 4–6 for the Cu and Ni films with 200 nm of thickness, respectively, indicates that the different free energy values of the two metals probably influenced the final aspects of the deposited films; that is, the free energy of Ni (2364 J/m^2) favored the formation of a texture denser and a more compact film, also, the lower free energy of Cu (1934 J/m^2) resulted in a surface with more voids (Himpel *et al.* 1998).

Probably, the growth of the Cu and Ni nanofilms occurred according to Volmer–Weber model, which considers a greater interaction between adjacent metal atoms in the film in relation to the metal-substrate interaction. This model results in the stable growth of tridimensional clusters on the substrate surface, which coalesce when neighbor islands result in free spaces (voids) among the coalesced islands (Cordill *et al.* 2022; Hora *et al.* 2018; Ohring 2001).

XRD and EDS

Figure 7 shows the X-ray diffractograms of PET substrate, the metallic thin films, and the EDS results of samples. XRD diffractogram of PET substrate presented peaks at 2θ equal to 22.8° and 25.8° , according to CPDS 00-061-1413. Already, the XRD patterns of the metallic nanometric films showed peaks related to the PET substrate, and also other contributions ranging from 35° and 70° , which confirm the deposition of metallic films on the polymeric substrate. The films obtained by the sputtering of Cu show the presence of copper oxide (Cu_2O) with contributions at 42.5° , 46° , and 53.8° (CPDS 00-035-1091, crystalline system not defined). A similar behavior was observed for the Ni film, which shows peaks related to nickel oxide (NiO) with contributions at 37° , 43° , and 62.5° (CPDS 00-071-4750, cubic system). Fig. 7a also shows a contribution at 45.8° angle, identified as $\text{NiO}_{0.75}\text{CuO}_{0.25}$ oxide (CPDS 01-8057-69), more intense in the copper films. The occurrence of this mixed oxide probably occurred due to the remaining presence of Ni and Cu vapor, originating from the preliminary step carried out to adjust the deposition parameters in the chamber. In both cases, contributions related to the pure metals were not observed. These results show that the films produced have a superficial layer of metallic oxide on the surface of the polymeric film, due to their inherent tendency to form oxides when in contact with oxygen. EDS analyses corroborate the XRD results and confirm the presence of the metals and oxygen on the surface of the metallic nanometric films. The presence of nitrogen on the surfaces of the metallic films was neglected to facilitate the interpretations of the XRD patterns. EDS results show an increase in oxygen concentration in metallic films with a thickness of 65 nm (34.9 – 36.3%) compared to PET (26.2%), showing the oxidation of the metallic surface. Proportionally, the 200 nm films have a lower concentration of oxygen (12.5 – 20.3%), but considering the mass proportion of metal in both films, these values are expected and they indicate the presence of oxides on surfaces.



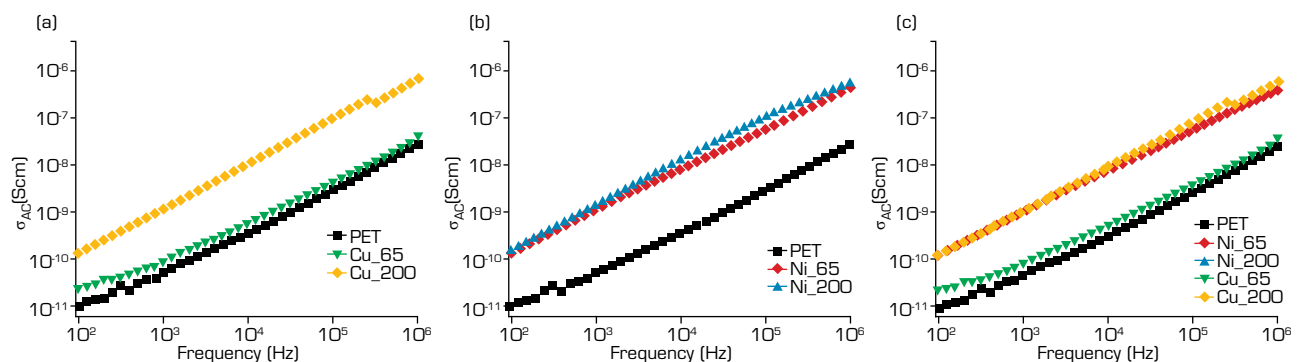
Source: Elaborated by the authors.

Figure 7. XRD (a) and EDS (b) results of PET and the films of Cu and Ni with 65 and 200 nm of thickness.

Electrical characterization

The AC electrical conductivity behaviors of the metallic thin films with different thicknesses (65 and 200 nm), as well as the PET substrate, were measured at room temperature by the two-point probe method. Figure 8 shows that the AC electrical conductivity of the PET substrate and metallic thin films increases as the frequency increases.

The PET substrate presents the lowest AC conductivity as a function of the frequency band, as expected, ranging from 1.0×10^{-11} to 1.0×10^{-8} S/cm, considering its electrical insulating behavior. In a general way, all metallic thin films present higher AC electrical conductivity compared to PET, which confirms the metallic deposition of Cu and Ni on the polymeric substrate. However, the AC conductivity values are still low. Figure 8a shows distinct behaviors for the AC conductivity curves of the Cu films with the two different thicknesses, but both ranging from $\sim 10^{-11}$ to $\sim 10^{-6}$ S/cm. Figure 8b shows AC conductivity curves of the Ni thin films, which are practically superimposed for the samples with different thicknesses, with values varying from $\sim 10^{-10}$ to $\sim 10^{-6}$ S/cm. The slight increase in the electrical conductivity of all thin films (Fig. 8c) compared to the PET ones can be attributed to the insulating oxides formed on the surface of metallic films, as shown in XRD and EDS analyses. The lowest increase observed for the Cu_65 nm film also suggests the presence of more defects in this sample.



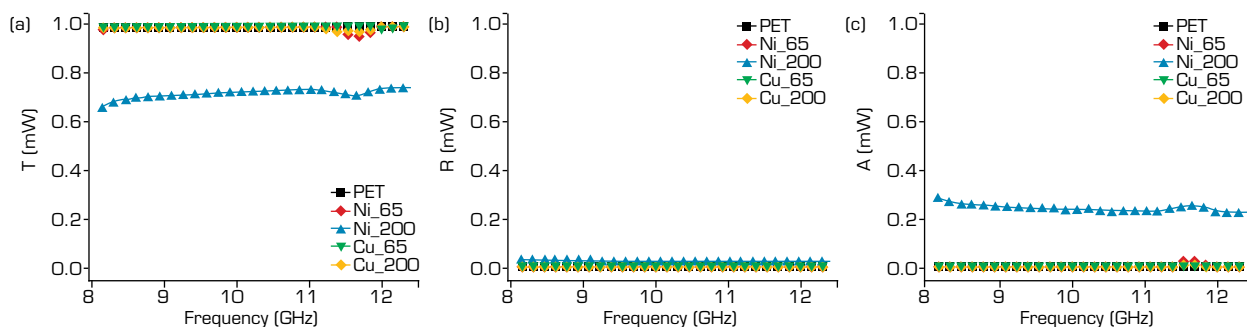
Source: Elaborated by the authors.

Figure 8. Total AC volumetric conductivity of PET and the metallic thin films of Cu (a); Ni (b); and the comparison of all AC curves (c).

EM characterization

Figure 9 shows the power balance for the PET substrate and the Cu and Ni nanometric films with different thicknesses, with the reflection (R), absorption (A), and transmission (T) coefficients as a function of the frequency range (8.2 – 12.4 GHz). Figure 9a shows that the PET substrate is predominantly transparent in all frequency range, with the neglected contribution of reflection

(Fig. 9b) and absorption (Fig. 9c). This is due to no charge carriers in the PET polymer, which make it highly transparent to microwaves (Chandra *et al.* 2023). This behavior is recommended for a substrate with thin films, as it avoids possible influences on the deposited film. Opposite behavior was observed in the magnetic properties of polycrystalline $\text{Zn}_{1-x}\text{Mn}_x\text{O}$ films synthesized on glass and p-type Si substrates using sol-gel technique. The authors observed that films grown on glass substrates did not exhibit ferromagnetic behavior even after heat treatment. In contrast, $\text{Zn}_{1-x}\text{Mn}_x\text{O}_3$ films grown on Si substrate exhibited ferromagnetic properties after heat treatment (Mikailzade *et al.* 2021). The use of a polymeric substrate, when possible, is advantageous because its inert and electrically insulating characteristics have a negligible influence on the deposited film.



Source: Elaborated by the authors.

Figure 9. Curves of Transmission (a); Reflection (b); and Absorption (c); coefficients as a function of frequency for the Cu and Ni thin films with different thicknesses.

The Cu and Ni thin films show similar behavior of the PET substrate with predominant transparent behavior in all frequency range analysed, and low reflection and absorption, except for the Ni₂₀₀ thin film. In the case of this sample, the transmission of EM wave was close to 0.7 mW, the reflection began at 0.035 mW at 8.2 GHz with a slight decrease until ~0.022 mW at 12.4 GHz, and absorption close to 0.25 mW in the X-band. This behavior shows that the thickness increase of the Ni film blocks part of the EM wave transmission through the film due mainly to the absorption phenomenon. It is also observed that the ability of this film to transform electromagnetic radiation into heat is practically independent of frequency since the absorption is approximately constant in all frequency range. This behavior characterizes the Ni₂₀₀ film as a broadband absorber.

At the same time that the AC electrical conductivity behavior of the nanometric films shows the trend of increasing values with the frequency increase, it is observed that the Ni₆₅, Ni₂₀₀, and Cu₂₀₀ samples show very close results of R, T, and A. This behavior suggests that the electrical conductivity does not show a significant influence on the absorption behavior. Based on this result, the performance observed for Ni₂₀₀ thin film can have been more strongly influenced by the morphological aspects of its surface, which can be contributed for more mechanisms of energy losses, for example, by interfacial polarization among the islands formed.

Table 3 shows the values T, R, and A coefficients, complex electrical permittivity and magnetic permeability, and the loss tangents values, at 10 GHz. T, R, and A coefficients, at 10 GHz, confirm the transparent behavior of the PET substrate and also the Cu film with 65 and 200 nm thickness, and the Ni film with 65 nm. On the other hand, it can be observed the less transparent behavior for the Ni₂₀₀ thin film and its more intense absorption behavior.

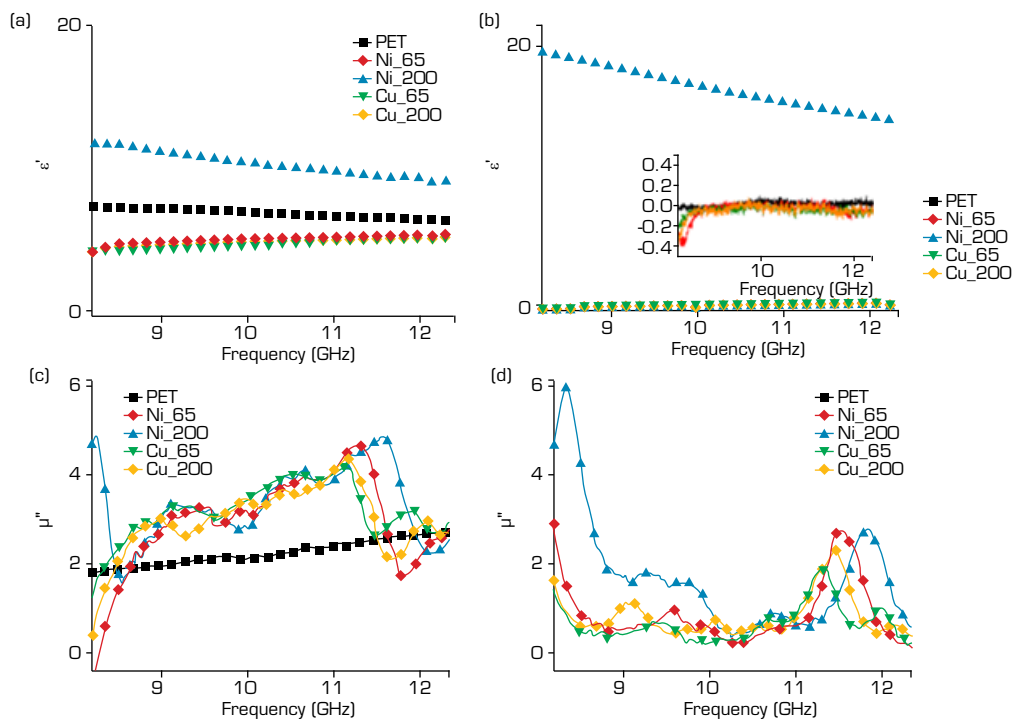
The absorption and reflector behaviors of materials are dependent on the electrical permittivity (ϵ) and magnetic permeability (μ) parameters. The real part of these components (ϵ' and μ') represents the interaction of the electrical and magnetic fields, respectively, of the EM wave with the material. Furthermore, the imaginary components (ϵ'' and μ'') represent the energy losses (Kaiser 2004; Wang *et al.* 2021b). Table 3 shows these components at 10 GHz and Fig. 10 shows the curves of ϵ and μ parameters in the X-band.

It is observed that the PET substrate and the Cu thin films with 65 and 200 nm, and the Ni₆₅ show ϵ' values varying between 4.2605 and 4.8712, at 10 GHz (Table 2). The ϵ' values for PET are relatively high for a polymeric substrate, compared to other polymers (Reis *et al.* 2022), but this behavior can be attributed to the molecular structure of PET, consisting of aromatic rings, conjugated bonds, and ester groups. These molecular characteristics probably favored a greater interaction of the polymer with the electrical field of the EM wave, but with low losses (low ϵ''). In addition, Table 2 shows values close to ϵ' for Cu and Ni₆₅ metallic thin films compared to PET.

Table 3. Values of A, R, and T parameters and the complex parameters of ϵ and μ , at 10 GHz, for the Cu and Ni thin films.

Samples	Potency (mV)			Permittivity			Permeability		
	R	T	A	ϵ'	ϵ''	ϵ''/ϵ'	μ'	μ''	μ''/μ'
PET	0.0008	0.9960	0.0032	4.2605	-0.0360	-0.0084	1.9598	0.2043	0.1042
Cu_65	0.0005	0.9942	0.0052	4.5103	0.0167	0.0037	3.4491	0.2300	0.0667
Cu_200	0.0007	0.9886	0.0108	4.6648	0.0363	0.0078	3.4836	0.6165	0.1770
Ni_65	0.0009	0.9882	0.0109	4.8712	0.0269	0.0055	3.1915	0.5814	0.1822
Ni_200	0.0247	0.7238	0.2515	10.3298	17.2287	1.6679	3.5637	0.5157	0.1447

Source: Elaborated by the authors.



Source: Elaborated by the authors.

Figure 10. Curves of ϵ' (a), ϵ'' (b), μ' (c), and μ'' (d) as a function of frequency for the Ni and Cu thin films with different thicknesses.

On the other hand, the Ni_200 thin film presents a higher value of ϵ' (10.3298, at 10 GHz), which suggests a better interaction of this sample with the EM wave, probably due to a greater structural homogeneity, with increasing crystallite size and more dense nanocrystals, that contributed to increase the degree of polarization, resulting in higher losses ($\epsilon''/\epsilon' = 1.6679$). It is also observed that ϵ' of the Ni_200 thin film shows a more accentuated decrease with the increasing frequency. According to Koop's theory, this behavior can be understood by considering the material as composed of well-conducting grains that are surrounded by poorly conductive grain boundaries (Saleem *et al.* 2020). The confirmation of this discussion was hampered by the XRD patterns obtained, which only detected the presence of oxides on the surface of films, without showing the formation of the crystalline phase of pure metals (Cu and Ni).

However, the analysis of ϵ'' in the Ni_200 thin film shows an anomalous and unexpected behavior; that is, the ϵ'' is higher than the real component (ϵ'). First, this unexpected result seems wrong, but repetitive analyses of different samples of the same film

confirmed this behavior. Then this result suggested that the EM wave absorbed by the film promoted other loss mechanisms, for example, parasite currents (Eddy currents) (Perez 2018; Wang *et al.* 2015), electrical dipoles, and metal/metal interface polarization (Wang *et al.* 2021c), which increased ϵ'' . The literature cites similar behavior for permeability, attributing this behavior to losses by natural resonance, Eddy current, and interfacial polarization along the boundaries of particles (Yin *et al.* 2018; 2019).

The analysis of the magnetic parameters (Table 3) shows that the metallic films have higher values of μ' (3.1915 - 3.5637) compared to PET (1.9598), which confirms the metal deposition on the polymeric substrate and also indicates the interaction of the magnetic field of the EM wave with the thin films. The literature shows studies exploring the high performance of microwave absorbers, focusing on reducing the reflected wave from the air-absorber interface by improving the impedance matching (Han *et al.* 2015), increasing the complex permeability (Li *et al.* 2010), reducing the complex permittivity (Wang *et al.* 2012a), or depositing resistive film with 377 Ω (Wang *et al.* 2012b). In accordance with the literature, the samples studied in the present work involved improved impedance matching by increasing the permeability by the deposition of metallic thin films.

The ϵ''/ϵ' (dielectric loss tangent, or $\tan \delta_\epsilon$) and μ''/μ' (magnetic loss tangent, or $\tan \delta_\mu$) (ratios) are related to the attenuation capacity of dielectric and magnetic RAM. Consequently, the values of $\tan \delta_\epsilon$ and $\tan \delta_\mu$ should be as high as possible, although the impedance should be close to the free space impedance to achieve no reflection on the front surface of the material (Saleem *et al.* 2020). Despite the low permeability values, the magnetic loss tangent is more expressive than dielectric loss tangent for the PET and the thin films of Cu (all) and the Ni_65. This result suggests that the magnetic losses have some contribution to the small absorption presented by these samples. On the other hand, the Ni_200 film shows that the losses occur predominantly by dielectric mechanisms ($\epsilon''/\epsilon' = 1.6679$).

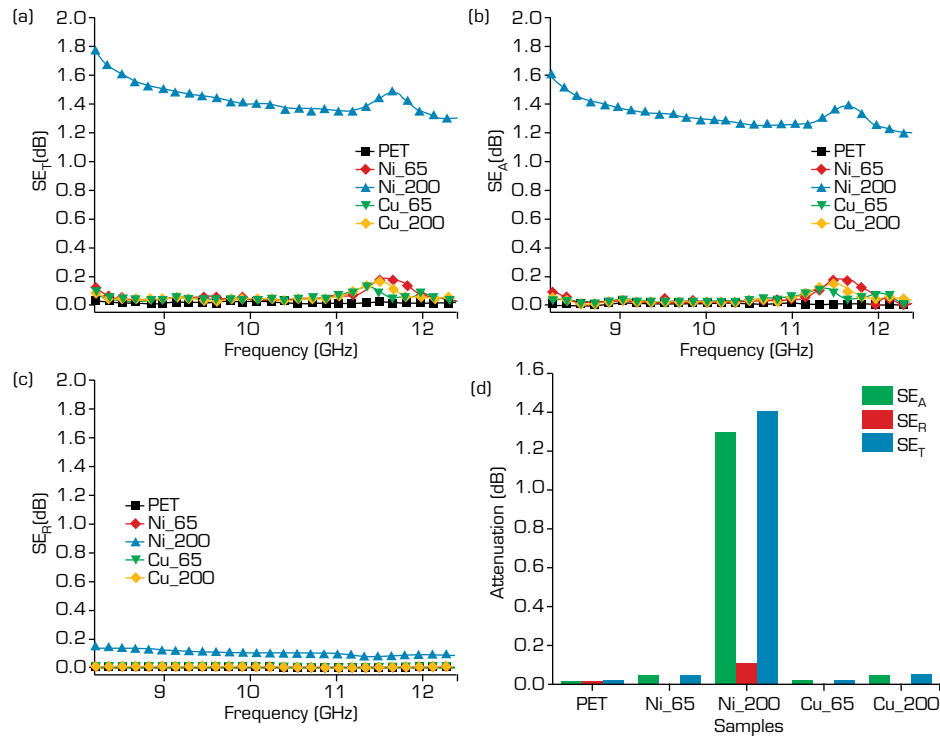
Table 3 summarizes the dielectric loss tangent (ϵ''/ϵ') at 10 GHz for the PET substrate and the Cu_65, Cu_200, and Ni_65 thin films with values close to zero. However, these samples show some magnetic losses. These results reveal that the magnetic losses are more significant than the dielectric ones. On the other hand, the Ni_200 film shows an ϵ''/ϵ' value that stands out compared to the others and that is also higher than the μ''/μ' . These values indicate that the dielectric loss tangents are more significant than the magnetic ones for this sample.

According to the literature, when one electrical field is applied, several electric dipoles are formed in the dielectric material (thin film) (Naghdi *et al.* 2018; Soethe *et al.* 2011). The interaction between the dipoles and the electric field leads to the formation of aligned dipoles according to the applied electric field, allowing the material to store electric energy (Folgueras and Rezende 2007; Ruiz-Perez *et al.* 2022). Considering this dielectric characteristic and analyzing the AFM image of the Ni_200 film, it is possible to consider that the more complex symmetrical nanostructure of this sample, composed of a finer texture with nano peaks in a certain order, the absorption of the EM wave was increased. The literature discusses a similar behavior for a complex symmetrical nanostructure of CuS in polyvinylidene fluoride (PVDF) nanocomposites with enhanced absorption properties (He *et al.* 2013). Based on this literature, it can be assumed that the nanostructure of Ni_200 thin film can favor interfacial polarization, caused by the dangling band atoms on the surface of nanostructures with complex geometric symmetry.

The effect of absorption and reflection on the power balance of the thin films reflects also on the shielding effectiveness (SE) behavior. The shielding effectiveness of a material is the capacity to attenuate EM radiation that can be expressed in terms of incident and transmitted power. The total shielding effectiveness (SE_T) of a material can be obtained by a sum of its absorption (SE_A) and reflection (SE_R), according to Eqs. 7–9 (Wang *et al.* 2021b). It is worth mentioning that the multiple internal reflections (SE_M) is related to the losses by multiple reflections inside the material, which can be neglected if SE_T is higher than 15 dB (Kumar, 2019; Reis *et al.* 2022). In the present work, the SE_M was neglected, considering the predominant transparent behavior of samples.

Figure 11 shows the correlation of SE as a function of increased frequency and it is observed that the PET substrate, the Ni_65, Cu_65, and Cu_200 thin films do not contribute to the SE, with values close to zero. So, the EMI SE of the Cu (65 and 200 nm) and the Ni thin films with 65 nm thickness can be neglected because these samples are predominantly transparent, similar to the PET substrate behavior. Already, the Ni_200 thin film shows better shielding properties ($SE_T = 1.4$ dB or $\sim 30\%$) (Fig. 11a). This value is not suitable for practical applications (>20 dB) (Anjos *et al.* 2023; Gama and Rezende 2010; Luo *et al.* 2023; Reis *et al.* 2022), but it is indicative that new increments of thickness or the combination of this film with others in a sandwich structure may result in more promising results. On the other hand, the Ni_200 thin film shows SE in the entire frequency range studied

(broadband behavior), with contributions of absorption (SE_A) (Fig. 11b) and reflection (SE_R) (Fig. 11c), although they are low. Figure 11a shows SE_T with broadband behavior and values ranging from 1.3 to 1.8 dB, in the X-band. These values correspond to (~23 – 30) % of attenuation of the incident wave. Figure 11d shows that the Ni_200 thin film presented an improved impedance matching, which favored absorption as the dominating mechanism in microwave attenuation.



Source: Elaborated by the authors.

Figure 11. Values of SE_T (a), SE_A (b), and SE_R (c) in function of frequency and histograms of SE_R , SE_A , and SE_T , at 10 GHz, (d) for the nanofilms.

Theoretical models show that the low thickness and the increased resistivity are responsible for the electron scattering at the film surface and the electron scattering at the grain boundaries of films (Ruvinskii *et al.* 2016). However, in the case of thin films, due to the quantum processes of interaction of the incident electromagnetic wave with the electronic structure of the film material, the absorption of radiation is a direct consequence of the presence of defects and high resistivity. Thus, metallic thin films become interesting in RAM manufacturing, because they are capable of dissipating EM waves by their conversion into heat.

CONCLUSION

Nanometric films of Cu and Ni were successfully produced with thickness values of 65, and 200 nm, by the magnetron sputtering technique. FEG-SEM and AFM analyses showed that the nanofilms of Cu and Ni presented different textures due, probably, to the different free energy of both metals. The observed texture suggests that the nanofilms were grown according to the Volmer–Weber model. The Ni film surface is denser, finer, and more compact compared to the Cu films, which present more voids among the islands formed. XRD analyses showed that both families of nanofilms have oxides on the surface, which decreased the electrical conductivity values that were relatively low for all samples studied. Electromagnetic characterization in the X-band shows that the Cu and Ni thin films have low performance in electromagnetic shielding, except the Ni film with 200 nm that showed more promising results with values close to 30% of attenuation in broadband, due to more prominent dielectric losses. The loss mechanisms observed in the studied thin films are mainly attributed to interfacial polarization and also to Eddy current loss and ohmic losses. The results presented in this study show the viability of producing new broadband absorbers that can work in broadband, with reduced thickness (nanometric), and with very light-weight.

CONFLICT OF INTEREST

Nothing to declare.

AUTHORS' CONTRIBUTIONS

Conceptualization: Gonçalves VFM, Nohara EL, Rezende MC; **Formal analysis:** Gonçalves VFM, Rezende MC; **Acquisition of funding:** Rezende MC; **Research:** Gonçalves VFM, Nohara EL, Rezende MC; **Methodology:** Gonçalves VFM, dos Anjos EGR, Morgado GFM, Brazil TR, Baldan MR, de Souza MAM, Nohara EL, Rezende MC; **Supervision:** Nohara EL, Rezende MC; **Writing - Preparation of original draft:** Gonçalves VFM, Rezende MC; **Writing - Proofreading and editing:** Gonçalves VFM, Rezende MC.

DATA AVAILABILITY STATEMENT

The data will be available upon request.

FUNDING

Conselho Nacional de Desenvolvimento Científico e Tecnológico
[<https://doi.org/10.13039/501100003593>]
Grant No: 305123/2018-1

ACKNOWLEDGEMENTS

To Prof. Dr. Marli Leite de Moraes for the support in the AFM analyses.

REFERENCES

- Abdumutalibovich NK (2021) Study of the technology of obtaining thin films in the field of microelectronics. *IJDPP* 1(4):51-53.
- Abhishek K, Singh S (2018) Development of Coatings for Radar Absorbing Materials at X-band. *IOP Conf Ser: Mater Sci Eng* 330:012006. <https://doi.org/10.1088/1757-899X/330/1/012006>
- Al-Saleh MH, Al-Anid HK, Husain YA, El-Ghanem HM, Jawad AS (2013) Impedance characteristics and conductivity of CNT/ABS nanocomposites, *J Phys D: Appl Phys* 46(38):385305. <https://doi.org/10.1088/0022-3727/46/38/385305>
- Anjos EGR, Brazil TR, Morgado GFM, Montagna LS, Braga NF, Antonelli E, Marini J, Rezende MC, Passador FP (2023) Influence of MWCNT aspect ratio on the rheological, electrical, electromagnetic shielding, and mechanical properties of polycarbonate melt mixed nanocomposites. *J Polym Res* 30:89. <https://doi.org/10.1007/s10965-023-03453-8>
- Bhat KS, Datta SK, Suresh C (1998) Electrical and Microwave Characterization of Kanthal Thin Films: Temperature and Size Effect. *Thin Solid Films* 332(1-2):220-224. [https://doi.org/10.1016/S0040-6090\(98\)01103-1](https://doi.org/10.1016/S0040-6090(98)01103-1)

- Biscaro RS, Rezende MC, Faez R (2008) Influence of doped polyaniline on the interaction of PU/PAni blends and on its microwave absorption properties. *Polym Adv Technol* 19(2):151-158. <https://doi.org/10.1002/pat.990>
- Bregar VB (2004) Advantages of ferromagnetic nanoparticle composites in microwave absorbers. *IEEE Trans Magn* 40(3):1679-1684. <https://doi.org/10.1109/TMAG.2004.826622>
- Chandra RBJ, Shivamurthy B, Kumar MS, Prabhu NN, Sharma D (2023) Mechanical and Electrical Properties and Electromagnetic-Wave-Shielding Effectiveness of Graphene-Nanoplatelet-Reinforced Acrylonitrile Butadiene Styrene Nanocomposites. *J Compos Sci* 7(3):117. <https://doi.org/10.3390/jcs7030117>
- Cordill MJ, Kreiml P, Mitterer (2022) Materials Engineering for Flexible Metallic Thin Film Applications. *Materials* 15(3):926. <https://doi.org/10.3390/ma15030926>
- Costa DS, Nohara EL, Rezende MC (2017) Comparative study of experimental and numerical behaviors of microwave absorbers based on ultrathin Al and Cu films. *Mater Chem Phys* 194:322-326. <https://doi.org/10.1016/j.matchemphys.2017.03.056>
- Dias JC, Martin IM, Rezende MC (2012) Reflectivity of Hybrid Microwave Absorbers Based on NiZn Ferrite and Carbon Black. *J Aerosp Technol Manag* 4(3):267-274. <https://doi.org/10.5028/jatm.2012.04032512>
- Folgueras LC, Rezende MC (2007) Hybrid Multilayer Structures for use as Microwave Absorbing Material. Paper presented at: 2007 SBMO/IEEE MTT-S International Microwave and Optoelectronics Conference; Salvador, Brazil. <https://doi.org/10.1109/IMOC.2007.4404310>
- Fontana LC, Muzart JLR (1998) Characteristics of Triode Magnetron Sputtering: the Morphology of Deposited Titanium Films. *Surf Coat Technol* 107(1):24-30. [https://doi.org/10.1016/S0257-8972\(98\)00576-3](https://doi.org/10.1016/S0257-8972(98)00576-3)
- Gama AM, Rezende MC (2010) Complex permeability and permittivity variation of carbonyl iron rubber in the frequency range of 2 to 18 GHz. *J Aerosp Technol Manag* 2(1):59-62. <https://doi.org/10.5028/jatm.2010.02015962>
- Goktas A (2018) High-quality solution-based Co and Cu co-doped ZnO nanocrystalline thin films: Comparison of the effects of air and argon annealing environments. *J Alloys Compd* 735:2038-2045. <https://doi.org/10.1016/j.jallcom.2017.11.391>
- Goktas S, Goktas A (2021) A comparative study on recent progress in efficient ZnO based nanocomposite and heterojunction photocatalysts: A review. *J Alloys Compd* 863:158734. <https://doi.org/10.1016/j.jallcom.2021.158734>
- Han R, Li W, Zhu M, Li F (2015) An enhancement of reflection loss by controlling the reflected electromagnetic wave at air-absorber interface. *Appl Phys A* 119(1):201-204. <https://doi.org/10.1007/s00339-014-8948-4>
- Hashsish EA (2002) Design of Wideband Thin Layer Planar Absorber. *J Electromagn Waves Appl* 16(2):227-241. <https://doi.org/10.1163/156939302X00868>
- He S, Wang G-S, Lu C, Liu J, Wen B, Liu H, Guo L, Cao M-S (2013) Enhanced wave absorption of nanocomposites based on the synthesized complex symmetrical CuS nanostructure and poly(vinylidene fluoride). *J Mater Chem A* 1(15):4685-4692. <https://doi.org/10.1039/c3ta00072a>
- Himpel FJ, Ortega JE, Mankey GJ, Willis RF (1998) Magnetic nanostructures. *J Adv Phys* 47(4):511-597. <https://doi.org/10.1080/000187398243519>
- Hora J, Hall C, Evans D, Charrault E (2018) Inorganic thin film deposition and application on organic polymer substrates. *Adv Eng Mater* 20(5):1700868. <https://doi.org/10.1002/adem.201700868>
- Hsu K-C, Chen J-Y, Fang T-H, Lin M-H (2018) Size-dependent strength and interface-dominated deformation mechanisms of Cu/Zr multilayer nanofilms. *Results Phys* 11:684-689. <https://doi.org/10.1016/j.rinp.2018.10.010>

Kaiser KL (2004) *Electromagnetic Compatibility Handbook*. Boca Raton: CRC Press.

Kumar N, Vadera SR (2017) *Stealth Materials and Technology for Airborne Systems*. In: Prasad N, Wanhill R, editors. *Aerospace Materials and Material Technologies*. Indian Institute of Metals Series. Singapore: Springer. p.519-537. https://doi.org/10.1007/978-981-10-2134-3_24

Kumar P (2019) Ultrathin 2D Nanomaterials for Electromagnetic Interference Shielding. *Adv Mater Interfaces* 6(24):1901454. <https://doi.org/10.1002/admi.201901454>

Li ZW, Yang ZH, Kong LB (2010) Ultrabroad bandwidth of single-layer electromagnetic attenuation composites with flaky fillers. *Appl Phys Lett* 96(9):092507. <https://doi.org/10.1063/1.3340460>

Luo S, Peng L, Xie Y, Cao X, Wang X, Liu X, Chen T, Han Z, Fan P, Sun H, et al. (2023) Flexible large-area graphene films of 50–600 nm thickness with high carrier mobility. *Nano-Micro Lett* 15:61. <https://doi.org/10.1007/s40820-023-01032-6>

Marx VM, Toth F, Wiesinger A, Berger J, Kirchlechner C, Cordill MJ, Fischer FD, Rammerstorfer FG, Dehm G (2015) The influence of a brittle Cr interlayer on the deformation behavior of thin Cu films on flexible substrates: Experiment and model. *Acta Mater* 89:278-289. <https://doi.org/10.1016/j.actamat.2015.01.047>

Mikailzade F, Türkan H, Önal F, Zarbali M, Göktaş A, Tumbul A (2021) Structural and magnetic properties of polycrystalline Zn_{1-x}MnxO films synthesized on glass and p-type Si substrates using sol-gel technique. *Appl Phys A* 127:408. <https://doi.org/10.1007/s00339-021-04519-4>

Monti M, Zacccone M, Frache A, Torre L, Armentano I (2021) Dielectric spectroscopy of PP/MWCNT nanocomposites: Relationship with crystalline structure and injection molding condition. *Nanomaterials* 11(2):550. <https://doi.org/10.3390/nano11020550>

Naghdi S, Rhee KY, Hui D, Park SJ (2018) A review of conductive metal nanomaterials as conductive, transparent, and flexible coatings, thin films, and conductive fillers: Different deposition methods and applications. *Coatings* 8(8):278. <https://doi.org/10.3390/coatings8080278>

Nicolson AM, Ross GF (1970) Measurement of the intrinsic properties of materials by time domain techniques. *IEEE Trans Instrum Meas* 19(4):377-382. <https://doi.org/10.1109/TIM.1970.4313932>

Nie Y, He HH, Gong RZ, Zhang XC (2007) The electromagnetic characteristics and design of mechanically alloyed Fe-Co particles for electromagnetic-wave absorber. *J Magn Magn Mater* 310(1):13-16. <https://doi.org/10.1016/j.jmmm.2006.07.021>

Ohring M (2001) *Materials science of thin films*. San Diego: Academic Press.

Parucker VLS, Duarte DA, Parucker ML, Almeida ALA, Brustolin GE, Delatorre RG (2022) Titanium nanofilms applied as microwave absorber. *J Mater Res* 37(17):2862-2870. <https://doi.org/10.1557/s43578-022-00682-3>

Perez RJ (2018) *Handbook of Aerospace Electromagnetic Compatibility*. Hoboken: John Wiley & Sons. <https://doi.org/10.1002/9781119082880>

Pinto SS, Machado JPM, Gomes NAS, Rezende MC (2017) Influence of the aspect ratio of magnetic metallic additives on the microwave absorbing performance. *Mater Res Express* 4(9):96101. <https://doi.org/10.1088/2053-1591/aa8516>

Pinto, SS, Flipsen RC, Gomes NAS, Opelt CV, Rezende MC (2018) Morphological, electromagnetic and absorbing properties of PANI/epoxy resin samples. *J Polym Eng* 1(3):1. <https://doi.org/10.24294/jpse.v1i3.589>

Pinto, SS, Rezende MC (2018) Performance prediction of microwave absorbers based on POMA/carbon black composites in the frequency range of 8.2 to 20 GHz. *J Aerosp Technol Manag* 10:e1618. <https://doi.org/10.5028/jatm.v10.764>

- Pinto SS, Machado JPB, Gomes NAS, Rezende MC (2019) The influence of morphology, structure, and weight fraction of magnetic additives on the electromagnetic characteristics of composites. *J Magn Magn Mater* 484:126-138. <https://doi.org/10.1016/j.jmmm.2019.03.085>
- Putz B, Milassin G, Butenko Y, Völker B, Gammer C, Semprimoschnig C, Cordill MJ, (2017) Combined TEM and XPS studies of metal-polymer interfaces for space applications. *Surf Coat Technol* 332:368-375. <https://doi.org/10.1016/j.surfcoat.2017.07.079>
- Rajavel K, Luo S, Wan Y, Yu X, Hu Y, Zhu P, Sun R, Wong C (2020) 2D $Ti_3C_2T_x$ MXene/polyvinylidene fluoride (PVDF) nanocomposites for attenuation of electromagnetic radiation with excellent heat dissipation. *Compos Part A Appl Sci Manuf* 129:105693. <https://doi.org/10.1016/j.compositesa.2019.105693>
- Reis FC, Gomes NAS, Baldan MR, Ribeiro B, Rezende MC (2022) The influence of carbonyl iron and magnetite ferrite on the electromagnetic behavior of nanostructured composites based on epoxy resin/buckypapers. *J Magn Magn Mater* 563:170007. <https://doi.org/10.1016/j.jmmm.2022.170007>
- Rezende MC, Silva FS, Martin IM (2000) Materiais absorvedores de radiação eletromagnética. *Spectrum* 2:17-20.
- Ribeiro B, Gomes NAS, Rezende MC (2021) Lightweight multi-walled carbon nanotube buckypaper/glass fiber-epoxy composites for strong electromagnetic interference shielding and efficient microwave absorption. *J Mater Sci: Mater Electron* 32(11):14494-14508. <https://doi.org/10.1007/s10854-021-06007-0>
- Rojas JA, Santos LFP, Botelho EC, Ribeiro B, Rezende MC (2021) Morphological, mechanical, and electromagnetic interference shielding effectiveness characteristics of glass fiber/epoxy resin/ MWCNT buckypaper composites. *J Appl Polym Sci* 138(25):50589. <https://doi.org/10.1002/app.50589>
- Ruiz-Perez F, López-Estrada SM, Tolentino-Hernández RV, Caballero-Briones F (2022) Carbon-based radar absorbing materials: A critical review. *J Sci-Adv Mater Dev* 7(3):100454. <https://doi.org/10.1016/j.jsamd.2022.100454>
- Ruvinskii MA, Kostyuk OB, Dzundza BS, Makovyshyn VI (2016) The Influence of Surface on Scattering of Carriers and Kinetic Effects in n-PbTe Films. *J Phys Chem Solids* 17(4):520-526. <https://doi.org/10.15330/pcss.17.4.520-526>
- Saleem A, Zhang Y, Gong H, Majeed MK, Lin X, Hussain MM, Ashfaq MZ (2020) Electromagnetic wave absorption performance of Ni doped Cu-ferrite nanocrystals. *Mater Res Express* 7:016117. <https://doi.org/10.1088/2053-1591/ab6c1a>
- Silva WO, Ferreira CL (2019) Filmes Ultrafinos de Titânio Absorvedores de Micro-ondas. *RMCT* 36(1):26-29. [accessed May 14 2022]. <http://www.ebrevistas.eb.mil.br/CT/article/view/2778>.
- Silveira DC, Gomes NAS, Rezende MC, Botelho EC (2017) Electromagnetic Properties of Multifunctional Composites Based on Glass Fiber Prepreg and Ni/Carbon Fiber Veil. *J Aerosp Technol Manag* 9(2):231-240. <https://doi.org/10.5028/jatm.v9i2.657>
- Silveira DC, Gomes NAS, Rezende MC, Botelho EC (2020) Microwave absorbing properties of glass fiber/epoxy resin composites tailored with frequency selective surface based on nonwoven of carbon fibers metalized with nickel. *J Mater Sci: Mater Electron* 31(16):13095-13103. <https://doi.org/10.1007/s10854-020-03860-3>
- Soethe VL, Nohara EL, Fontana LC, Rezende MC (2011) Radar absorbing materials based on titanium thin film obtained by sputtering technique. *J Aerosp Technol Manag* 3(3):279-286. <https://doi.org/10.5028/jatm.2011.03030511>
- Vieira LS, Anjos EGR, Verginio GEA, Oyama IC, Braga NF, Silva TF, Montagna LS, Rezende MC, Passador FR (2021) Carbon-based materials as antistatic agents for the production of antistatic packaging: a review. *J Mater Sci: Mater Electron* 32(4):3929-3947. <https://doi.org/10.1007/s10854-020-05178-6>
- Wang T, Han R, Tan G, Wei J, Qiao L, Li F (2012a) Reflection loss mechanism of single layer absorber for flake-shaped carbonyl-iron particle composite. *J Appl Phys* 112(10):104903. <https://doi.org/10.1063/1.4767365>

Wang B, Wei J, Qiao L, Wang T, Li F (2012b) Influence of the interface reflections on the microwave reflection loss for carbonyl iron/paraffin composite backed by a perfect conduction plate. *J Magn Magn Mater* 324(5):761-765. <https://doi.org/10.1016/j.jmmm.2011.09.011>

Wang H, Li W, Feng Z (2015) Noncontact thickness measurement of metal films using Eddy-current sensors immune to distance variation. *IEEE Trans Instrum Meas* 64(9):2557-2564. <https://doi.org/10.1109/TIM.2015.2406053>

Wang B, Wu Q, Fu Y, Liu T (2021a) A review on carbon/magnetic metal composites for microwave absorption. *J Mater Sci Technol* 86:91-109. <https://doi.org/10.1016/j.jmst.2020.12.078>

Wang H, Li S, Liu M, Li J, Zhou X (2021b) Review on Shielding Mechanism and Structural Design of Electromagnetic Interference Shielding Composites. *Macromol Mater Eng* 306(6):2100032. <https://doi.org/10.1002/mame.202100032>

Wang M, Tang, X-H, Cai J-H, Wu H, Shen J-B, Guo S-Y (2021c) Construction, mechanism and prospective of conductive polymer composites with multiple interfaces for electromagnetic interference shielding: A review. *Carbon* 177:377-402. <https://doi.org/10.1016/j.carbon.2021.02.047>

Yadav R, Panwar R (2022) Multilayer gradient perforated radar absorbing structure for stealth applications in *IEEE Trans Magn* 58(2): 2800305. <https://doi.org/10.1109/TMAG.2021.3103133>

Yin P, Deng Y, Zhang L, Huang J, Li H, Li Y, Qi Y, Tao Y (2018) The microwave absorbing properties of ZnO/Fe₃O₄/paraffin composites in low frequency band. *Mater Res Express* 5:026109. <https://doi.org/10.1088/2053-1591/aaae58>

Yin P, Zhang L, Wang J, Feng X, Zhao L, Rao H, Wang Y, Dai J (2019) Preparation of SiO₂-MnFe₂O₄ Composites via One-Pot Hydrothermal Synthesis Method and Microwave Absorption Investigation in S-Band. *Molecules* 24(14):2605. <https://doi.org/10.3390/molecules24142605>